

Continuous-time multivariate analysis

Biplab Paul, Philip T. Reiss*

Department of Statistics, University of Haifa

and

Erjia Cui

Division of Biostatistics, University of Minnesota

January 15, 2024

Abstract

The starting point for much of multivariate analysis (MVA) is an $n \times p$ data matrix whose n rows represent observations and whose p columns represent variables. Some multivariate data sets, however, may be best conceptualized not as n discrete p -variate observations, but as p curves or functions defined on a common time interval. We introduce a framework for extending techniques of multivariate analysis to such settings. The proposed framework rests on the assumption that the curves can be represented as linear combinations of basis functions such as B-splines. This is formally identical to the Ramsay-Silverman representation of functional data; but whereas functional data analysis extends MVA to the case of observations that are curves rather than vectors — heuristically, $n \times p$ data with p infinite — we are instead concerned with what happens when n is infinite. We describe how to translate the classical MVA methods of covariance and correlation estimation, principal component analysis, Fisher’s linear discriminant analysis, and k -means clustering to the continuous-time setting. We illustrate the methods with a novel perspective on a well-known Canadian weather data set, and with applications to neurobiological and environmetric data. The methods are implemented in the publicly available R package `ctmva`.

Keywords: B-splines; correlation matrix; Fisher’s linear discriminant analysis; functional data; k -means clustering; principal component analysis

*The authors thank Hadar Fisher and Ciprian Crainiceanu for helpful discussions. The work of Paul and Reiss was supported by Israel Science Foundation under Grant 1076/19.

1 Introduction

The generic mathematical object that underpins much of multivariate analysis (MVA) is an $n \times p$ data matrix \mathbf{X} whose n rows represent observations and whose p columns represent variables. But some multivariate data sets may be best conceptualized not as n discrete p -variate observations, but as p curves or functions defined on a common time interval. This paper introduces a basis function framework for straightforwardly extending several techniques of multivariate analysis to this setting.

Heuristically, our proposed framework, henceforth *continuous-time multivariate analysis* (CTMVA), is the “transpose” of functional data analysis (FDA; Ramsay and Silverman, 2005), in the following sense. In a programmatic address that introduced the term “functional data” and foreshadowed the FDA paradigm, Ramsay (1982) argued that some modern data sets call for replacing the traditional p variables with infinitely many points on a continuum, as in the upper right picture in Figure 1, and suggested that spline methodology could play a key role in handling such infinite-dimensional data. He briefly noted that instead of taking $p = \infty$ as in FDA, one might consider situations in which $n = \infty$, as in the lower left picture in Figure 1; but he did not develop the $n = \infty$ case. The CTMVA framework is an attempt to do so, while maintaining an emphasis on the role of spline and other basis-function representations as in Ramsay (1982) and Ramsay and Silverman (2005).

To illustrate the contrast between CTMVA and FDA it may be instructive to reconsider what is perhaps the most famous example of functional data: the Canadian temperature data of Ramsay and Silverman (2005), consisting of mean temperatures on each day of the year at 35 weather stations in Canada. In FDA, these are viewed not as $n = 35$ observations of dimension $p = 365$, but as smooth curves $x_1(t), \dots, x_{35}(t)$ on $\mathcal{I} = [0, 365]$. Figure 2 displays both the raw data (upper panel) and the curves following roughness-penalty smoothing with respect to a 45-element Fourier basis (middle panel), with the smoothing parameter chosen by restricted maximum likelihood, as advocated by Ruppert et al. (2003) and Reiss and Ogden (2009) and implemented by Wood (2011). In CTMVA we again view the data as smooth curves $x_1(t), \dots, x_{35}(t)$, but these are now understood

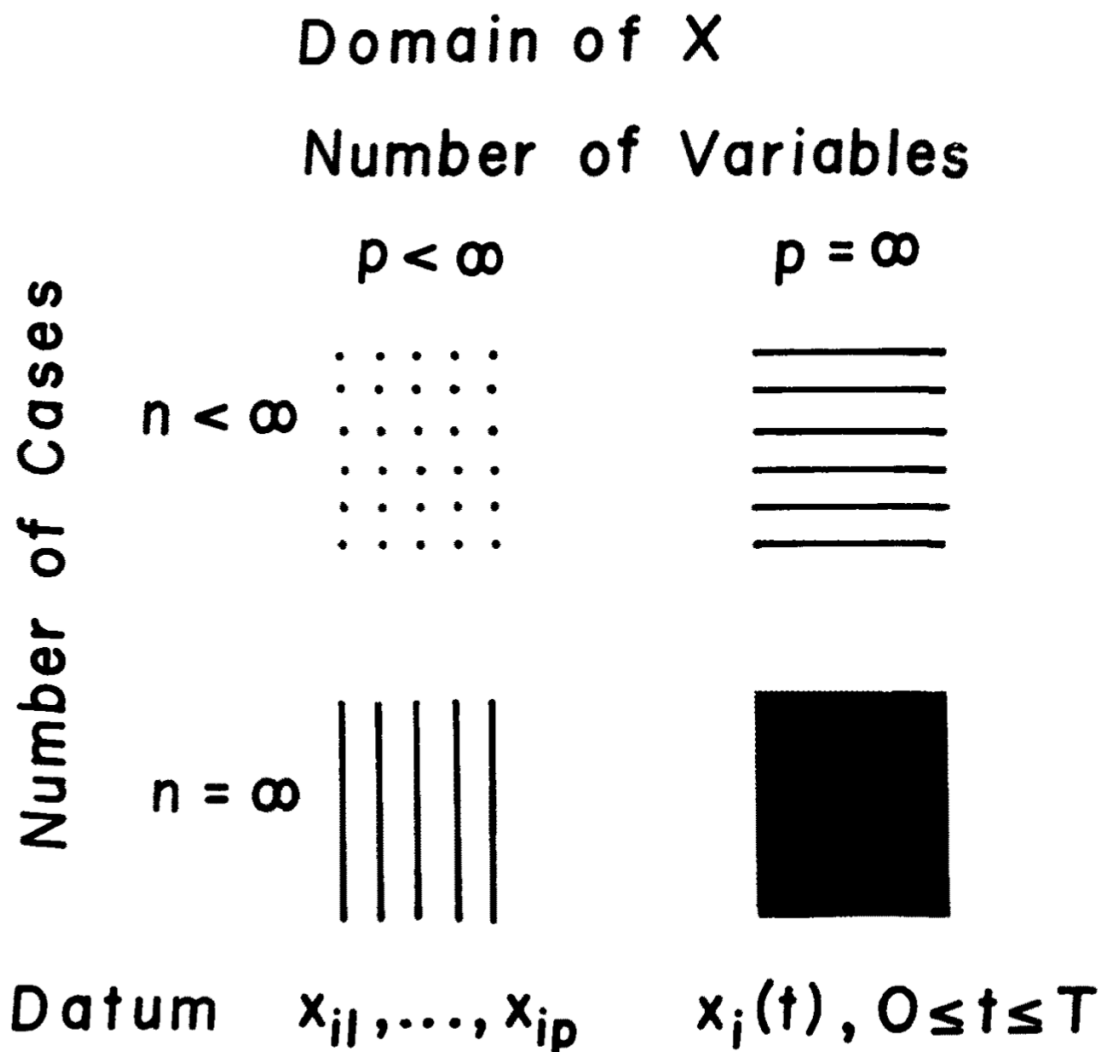


Figure 1: Schematic diagram presented by Ramsay (1982) to explain “the concept of a functional datum.” The diagram appeared as Figure 2 of that paper above the caption: “Possible domains for statistical observations. These domains depend on whether the number of replications or cases (n) is finite or infinite and whether the number of variables or points of observation (p) is finite or corresponds to the points on a continuum.” The upper right represents functional data, whereas the lower left scenario, mentioned but not developed by Ramsay (1982), is the continuous-time multivariate analysis setup of the present paper. Figure reproduced with permission from Springer Nature.

as $n = \infty$ observations of $p = 35$ variables.

In FDA, given a sample of curves arising from a stochastic process on a finite interval $\mathcal{I} \subset \mathbb{R}$, much interest focuses on $\Gamma(s, t)$, the covariance function of the underlying process. In particular, in functional principal component analysis one estimates the eigenfunctions of the associated covariance operator. In CTMVA, by contrast, the covariances or correlations of interest are those among the curves—representing, in this example, relationships among the various weather stations. For example, in §3 below we discuss the matrices shown at the bottom of Figure 2, representing correlations among the 35 stations’ temperature curves, and in §7.1 we consider correlations among precipitation curves from the same data set.

Following Ramsay and Silverman (2005), we make the fundamental simplifying assumption that, for $u = 1, \dots, p$, the u th function can be represented by means of an expansion $x_u(t) = \mathbf{c}_u^T \boldsymbol{\phi}(t)$ where $\boldsymbol{\phi}(t) = [\phi_1(t), \dots, \phi_K(t)]^T$ is a vector of *a priori* basis functions. Thus, if we define \mathbf{C} as the $K \times p$ coefficient matrix with u th column \mathbf{c}_u , then $\mathbf{x}(t) \equiv [x_1(t), \dots, x_p(t)]^T$ can be represented as

$$\mathbf{x}(t) = \mathbf{C}^T \boldsymbol{\phi}(t). \tag{1}$$

For the weather example it is natural to use a Fourier basis, which ensures fits that transition smoothly from December 31 to January 1; in most other examples we employ a B -spline basis. Our implementation of CTMVA in the R environment (R Core Team, 2023) depends on the B -spline and Fourier basis functions from the `fda` package for functional data analysis (Ramsay et al., 2009, 2023).

The practical impetus for CTMVA is twofold. First, representing a multivariate time series as a set of smooth curves, rather than a discrete set of observations, can sometimes improve performance of MVA techniques. Preliminary simulations establish this for correlation estimation, and we demonstrate this below for clustering, with the environmetric data analyzed in §7.3. Second, CTMVA can sometimes be applied when classical MVA cannot—for example, if the p variables are not measured at a uniform set of time points.

In §2 we define continuous-time versions of the sample mean vector and the sample covariance and correlation matrices. As part of this development, §3 clarifies the basic but possibly confusing role of centering, which can have an important effect on correlation esti-

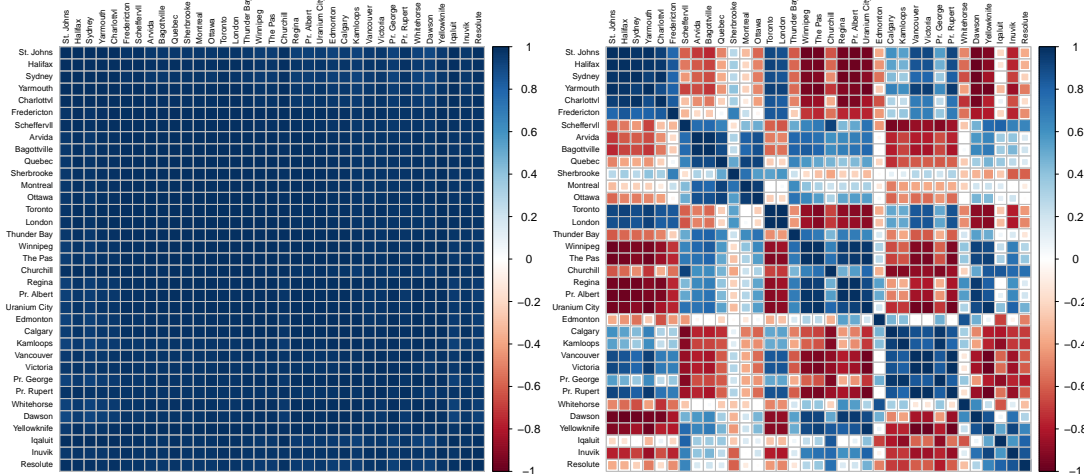
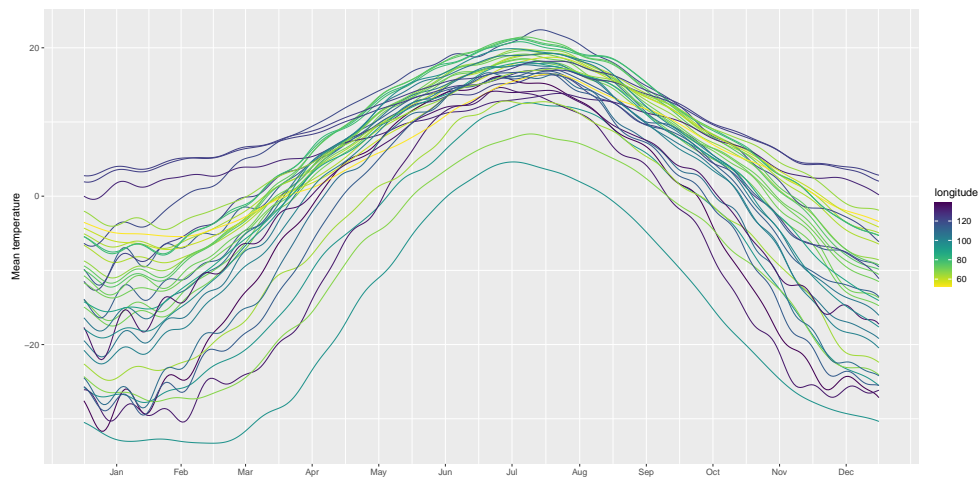
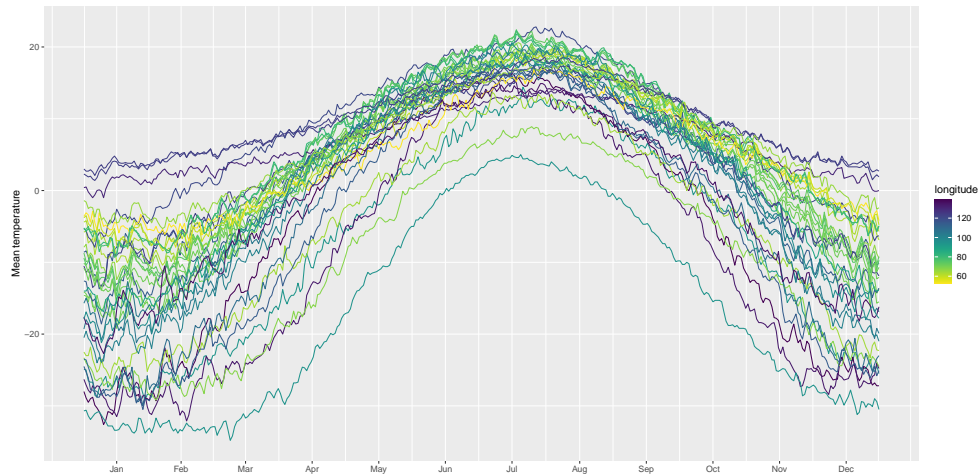


Figure 2: Top: Mean daily temperatures at 35 Canadian weather stations (Ramsay and Silverman, 2005). Middle: The same data after smoothing with respect to a Fourier basis. Below: Continuous-time correlations among daily mean temperatures in the 35 weather stations, visualized by the corrgram method (Friendly, 2002) implemented in Wei and Simko (2021), before (left) and after (right) removing the common seasonal trend.

mation. In §4–§6 we develop continuous-time (CT) versions of three key MVA techniques, namely principal component analysis, Fisher’s linear discriminant analysis and k -means clustering. Three real-data analyses are presented in §7. The paper concludes with a brief discussion in §8.

2 Continuous-time sample mean vector and covariance and correlation matrices

2.1 Definitions

The most basic CTMVA methods, which set the stage for much of what follows, are continuous-time analogues of the sample mean vector and sample covariance and correlation matrices. In classical multivariate analysis, given a data matrix $\mathbf{X} = (x_{ij})_{1 \leq i \leq n, 1 \leq j \leq p}$ representing n observations of a p -dimensional random vector, the p -dimensional sample mean vector and $p \times p$ covariance matrix are given, respectively, by $\bar{\mathbf{x}} = (\bar{x}_1, \dots, \bar{x}_p)^T$ with $\bar{x}_u = n^{-1} \sum_{i=1}^n x_{iu}$ and $\mathbf{S} = [\frac{1}{n} \sum_{i=1}^n (x_{iu} - \bar{x}_u)(x_{iv} - \bar{x}_v)]_{1 \leq u, v \leq p}$ [here we follow Mardia et al. (1979) in dividing by n rather than by $n - 1$].

The CT analogues of the mean vector and covariance matrix are derived by simply replacing sums of n observations divided by n with integrals over \mathcal{I} divided by the length of \mathcal{I} , leading to the CT mean vector

$$\bar{\mathbf{x}}^* = (\bar{x}_1^*, \dots, \bar{x}_p^*)^T \quad \text{with} \quad \bar{x}_u^* = |\mathcal{I}|^{-1} \int_{\mathcal{I}} x_u(t) dt, \quad (2)$$

and the CT covariance matrix

$$\mathbf{S}^* = \left[|\mathcal{I}|^{-1} \int_{\mathcal{I}} [x_u(t) - \bar{x}_u^*][x_v(t) - \bar{x}_v^*] dt \right]_{1 \leq u, v \leq p} = |\mathcal{I}|^{-1} \int_{\mathcal{I}} [\mathbf{x}(t) - \bar{\mathbf{x}}^*][\mathbf{x}(t) - \bar{\mathbf{x}}^*]^T dt. \quad (3)$$

(Here and in what follows we use $*$ to signify CT analogues of classical MVA estimators.)

As in the classical case, the CT correlation matrix can be defined as

$$\mathbf{R}^* = \mathbf{D}^{*-1/2} \mathbf{S}^* \mathbf{D}^{*-1/2}, \quad (4)$$

where \mathbf{D}^* is the diagonal matrix with the same main diagonal as \mathbf{S}^* .

The continuous-time mean vector $\bar{\mathbf{x}}^*$ and covariance matrix \mathbf{S}^* can be easily derived as the limits, as $n \rightarrow \infty$, of their classical counterparts $\bar{\mathbf{x}}, \mathbf{S}$, when the rows of \mathbf{X} are $\mathbf{x}(t_1)^T, \dots, \mathbf{x}(t_n)^T$ where t_1, \dots, t_n form a grid of points on \mathcal{I} at equal intervals of $|\mathcal{I}|/n$ (e.g., $t_i = i/n$ for each i , for $\mathcal{I} = [0, 1]$). In that case $|\mathcal{I}|\bar{\mathbf{x}} = \frac{|\mathcal{I}|}{n} \sum_{i=1}^n \mathbf{x}(t_i)$ is a Riemann sum converging to $\int_{\mathcal{I}} \mathbf{x}(t) dt$ as $n \rightarrow \infty$; dividing by $|\mathcal{I}|$ yields $\bar{\mathbf{x}} \rightarrow \bar{\mathbf{x}}^*$. Consequently,

$$|\mathcal{I}|\mathbf{S} = \frac{|\mathcal{I}|}{n} \sum_{i=1}^n [\mathbf{x}(t_i) - \bar{\mathbf{x}}][\mathbf{x}(t_i) - \bar{\mathbf{x}}]^T \rightarrow \frac{|\mathcal{I}|}{n} \sum_{i=1}^n [\mathbf{x}(t_i) - \bar{\mathbf{x}}^*][\mathbf{x}(t_i) - \bar{\mathbf{x}}^*]^T,$$

and the latter expression is a Riemann sum converging to the matrix-valued integral in (3). Dividing by $|\mathcal{I}|$ leads to $\mathbf{S} \rightarrow \mathbf{S}^*$.

The basis representation (1) makes the integrals in (2), (3) computable even though $\mathbf{x}(t)$ is observed at only finitely many times t , and yields convenient and succinct expressions for $\bar{\mathbf{x}}^*$ and \mathbf{S}^* . Let $\bar{\boldsymbol{\phi}}^* = (\bar{\phi}_1^*, \dots, \bar{\phi}_K^*)^T$ where $\bar{\phi}_k^* = |\mathcal{I}|^{-1} \int_{\mathcal{I}} \phi_k(t) dt$, and define the $K \times K$ matrix

$$\mathbf{M} = \left[|\mathcal{I}|^{-1} \int_{\mathcal{I}} [\phi_k(t) - \bar{\phi}_k^*][\phi_\ell(t) - \bar{\phi}_\ell^*] dt \right]_{1 \leq k, \ell \leq K} = |\mathcal{I}|^{-1} \int_{\mathcal{I}} [\boldsymbol{\phi}(t) - \bar{\boldsymbol{\phi}}^*][\boldsymbol{\phi}(t) - \bar{\boldsymbol{\phi}}^*]^T dt. \quad (5)$$

Then $\bar{\mathbf{x}}^* = \mathbf{C}^T \bar{\boldsymbol{\phi}}^*$ and $\mathbf{S}^* = \mathbf{C}^T \mathbf{M} \mathbf{C}$. Details of how to compute $\bar{\boldsymbol{\phi}}^*$ and \mathbf{M} are provided in Appendix A.

2.2 Estimators or estimands?

In classical MVA, the sample mean $\bar{\mathbf{x}}$ is an estimate, based on independent observations $\mathbf{x}_1, \dots, \mathbf{x}_n$ from a common multivariate distribution, of the population mean $\boldsymbol{\mu} = E(\mathcal{X})$ of a random vector \mathcal{X} arising from that distribution. Similarly, the sample covariance matrix \mathbf{S} is an estimate of the population covariance matrix $\boldsymbol{\Sigma} = E[(\mathcal{X} - \boldsymbol{\mu})(\mathcal{X} - \boldsymbol{\mu})^T]$. In this regard, our setting is very different from the classical one, since instead of a sample of n independent observations, the entire function $\mathbf{x} : \mathcal{I} \rightarrow \mathbb{R}^p$ constitutes a single instance of a multivariate stochastic process on \mathcal{I} . Consequently, although we might view $\bar{\mathbf{x}}^*$ as an estimator of $\boldsymbol{\mu}^* \equiv |\mathcal{I}|^{-1} E[\int_{\mathcal{I}} \mathcal{X}(t) dt]$ for $\mathcal{X}(\cdot)$ generated from that process, and \mathbf{S}^* as an estimator of $\boldsymbol{\Sigma}^* \equiv |\mathcal{I}|^{-1} E[\int_{\mathcal{I}} \{\mathcal{X}(t) - \boldsymbol{\mu}^*\} \{\mathcal{X}(t) - \boldsymbol{\mu}^*\}^T dt]$, these estimates are based on a sample of only one (MV-function-valued) observation. Inference for the population quantities $\boldsymbol{\mu}^*, \boldsymbol{\Sigma}^*$

would require not one but multiple instances of the vector-valued function $\mathcal{X}(\cdot)$, and this will not be developed here; see Dubin and Müller (2005), who consider inference for a related notion of “dynamic correlation” in a population, based on a sample of instances of multivariate longitudinal data.

In many applications, such as those considered in this paper, interest centers not on the underlying MV stochastic process but on the specific instance $\mathbf{x}(\cdot)$. It is then more reasonable to regard $\bar{\mathbf{x}}^*$ and \mathbf{S}^* , along with \mathbf{R}^* , not as estimators but as estimands, since in practice the function $\mathbf{x}(\cdot)$ on which they are based is not observed perfectly, for three reasons: (i) the p component functions are observed only at finitely many time points, (ii) they are generally observed with noise and/or measurement error, and (iii) the basis representation (1) introduces approximation error. More formally, for $u = 1, \dots, p$, at finitely many times t_{iu} we observe not the true $x_u(t_{iu})$ but

$$z_{iu} = x_u(t_{iu}) + \varepsilon_{iu}, \quad (6)$$

where ε_{iu} represents zero-mean error. We apply penalized smoothing (Ruppert et al., 2003; Wood, 2017) to the z_{iu} 's for each u , to obtain estimates $\hat{\mathbf{x}}(t) = \hat{\mathbf{C}}^T \boldsymbol{\phi}(t) \in \mathbb{R}^p$ for the p functions. Thus $\bar{\mathbf{x}}^*$, \mathbf{S}^* , \mathbf{R}^* are unobservable but are estimated, respectively, by

$$\begin{aligned} \hat{\bar{\mathbf{x}}}^* &= |\mathcal{I}|^{-1} \int_{\mathcal{I}} \hat{\mathbf{x}}(t) dt = \hat{\mathbf{C}}^T \bar{\boldsymbol{\phi}}^*, & \hat{\mathbf{S}}^* &= |\mathcal{I}|^{-1} \int_{\mathcal{I}} [\hat{\mathbf{x}}(t) - \hat{\bar{\mathbf{x}}}^*][\hat{\mathbf{x}}(t) - \hat{\bar{\mathbf{x}}}^*]^T dt = \hat{\mathbf{C}}^T \mathbf{M} \hat{\mathbf{C}}, \\ \text{and } \hat{\mathbf{R}}^* &= \hat{\mathbf{D}}^{*-1/2} \hat{\mathbf{S}}^* \hat{\mathbf{D}}^{*-1/2}, \end{aligned} \quad (7)$$

where $\hat{\mathbf{D}}^*$ is the diagonal matrix with the same main diagonal as $\hat{\mathbf{S}}^*$. For simplicity, in what follows we omit the “hats” and treat \mathbf{x} and consequently $\bar{\mathbf{x}}^*$, \mathbf{S}^* , \mathbf{R}^* as given.

In simulations (in preparation), when data are generated from (6) at 500 time points after generating curve pairs $[x_1(t), x_2(t)]^T$ from a bivariate Gaussian process with between-curve correlation, we have found that the ordinary correlation \hat{r} tends to markedly underestimate the correlation $r^* = \frac{s_{12}^*}{s_1^* s_2^*}$ [see (4)] of the pair of curves. This bias is easy to explain: the noise term in (6) inflates variance without affecting between-curve covariance, resulting in diminished correlation. Such attenuation of correlation due to noise is a long-established phenomenon (e.g., Spearman, 1910) and is sometimes corrected by multiplying

the estimated correlation by the geometric mean of the two variables' reliabilities (Cohen et al., 2013). For time series as opposed to independent observations, such a correction is not straightforward to implement. But the CT approach proceeds by instead denoising the observed curves, resulting in correlation estimates \hat{r}^* that clearly outperform the ordinary correlation \hat{r} in estimating the between-curve correlation r^* . These preliminary simulation results, then, offer clear and concrete evidence for the benefits of CTMVA, even when ordinary MVA is feasible.

3 Two forms of centering

The mean-centered variable vector $\mathbf{x}^c(t) = \mathbf{x}(t) - \bar{\mathbf{x}}^*$ has already appeared in the covariance matrix (3) and has a number of other uses, such as for CT principal component analysis (see §4 below). The basis representation (1) implies that $\mathbf{x}^c(t) = \mathbf{C}^T[\boldsymbol{\phi}(t) - \bar{\boldsymbol{\phi}}^*]$, i.e. the centered variables are linear combinations of $\phi_1(t) - \bar{\phi}_1^*, \dots, \phi_K(t) - \bar{\phi}_K^*$, but it would be more convenient if we could represent them as linear combinations of the original (not centered) basis functions $\phi_1(t), \dots, \phi_K(t)$. It turns out that we can do so, under the simple condition that

$$\text{there exists } \mathbf{w} \in \mathbb{R}^K \text{ such that } \mathbf{w}^T \boldsymbol{\phi}(t) = 1 \text{ for all } t, \quad (8)$$

since then

$$\begin{aligned} \mathbf{x}^c(t) &= \mathbf{C}^T[\boldsymbol{\phi}(t) - \bar{\boldsymbol{\phi}}^*] \\ &= \mathbf{C}^T[\boldsymbol{\phi}(t) - \bar{\boldsymbol{\phi}}^* \mathbf{w}^T \boldsymbol{\phi}(t)] \\ &= \mathbf{C}^T[\mathbf{I}_K - \bar{\boldsymbol{\phi}}^* \mathbf{w}^T] \boldsymbol{\phi}(t), \end{aligned}$$

i.e., the centered data has a basis representation as in (1), but with coefficient matrix $[\mathbf{I}_K - \mathbf{w} \bar{\boldsymbol{\phi}}^{*T}] \mathbf{C}$ in place of \mathbf{C} . Condition (8) holds for B -spline bases, with $\mathbf{w} = (1, \dots, 1)^T$, and for Fourier bases, with $\mathbf{w} = (|\mathcal{I}|^{1/2}, 0, \dots, 0)^T$.

Centering in the above sense is the continuous-time version of column-centering an $n \times p$ data matrix. In some applications, a CT analogue of *row*-centering is warranted, i.e., a common trend $m(t) = \frac{1}{p} \sum_{u=1}^p x_u(t)$ should be subtracted from the p curves before

computing the covariance or correlation. Consider, for example, the Canadian temperature curves in Figure 2. Without removal of the common trend $m(t)$, the CT correlation matrix \mathbf{R}^* for this example has all elements above 0.9, since the temperatures at all stations are relatively high in the summer and low in the winter, yielding the uninformative correlation matrix in the lower left panel of Figure 2. But with detrending applied, the result is the more interesting correlation matrix in the lower right panel. The 35 stations are listed geographically, roughly from east to west, except for the last six stations, which are located in the Canadian North. The top and middle panels of Figure 2 suggest that in many cases, stations with nearly the same longitude have similar temperature curves. This explains why the CT correlation matrix has several blocks of very high positive correlations along the main diagonal: for instance, the first six stations are those located in the Atlantic provinces, and the correlations among them are all above 0.78 and mostly above 0.93.

In Appendix B we propose a simple diagnostic to help determine, for a given data set, whether detrending is advisable.

4 Principal component analysis

In classical MVA, the (sample) principal components are linear combinations $\mathbf{v}_1^T \mathbf{x}, \dots, \mathbf{v}_p^T \mathbf{x}$ that have maximal variance, subject to mutual orthonormality of the \mathbf{v}_j 's. If the sample covariance matrix \mathbf{S} has orthonormal eigenvectors $\mathbf{e}_1, \dots, \mathbf{e}_p$ with corresponding eigenvalues $\lambda_1 \geq \dots \geq \lambda_p$, then by a standard result on Rayleigh quotient maximization (e.g., Schott, 2017), the solution to this iterative optimization problem is $\mathbf{v}_m = \mathbf{e}_m$ for $m = 1, \dots, p$.

Continuous-time PCA seeks linear combination *functions* $\mathbf{v}_m^T \mathbf{x}(t)$ that achieve maximal variance in the above sense, but with the variance of $\mathbf{v}^T \mathbf{x}(t)$ defined as in (3) with respect to time, as

$$|\mathcal{I}|^{-1} \int_{\mathcal{I}} [\mathbf{v}^T \mathbf{x}^c(t)]^2 dt = \mathbf{v}^T \mathbf{S}^* \mathbf{v}. \quad (9)$$

Consequently, the solution is given not by the eigenvectors of \mathbf{S} , but by those of \mathbf{S}^* : $\mathbf{v}_m = \mathbf{e}_m^*$ for $m = 1, \dots, p$, where now $\mathbf{e}_1^*, \dots, \mathbf{e}_p^*$ are orthonormal eigenvectors of \mathbf{S}^* in descending order of the corresponding eigenvalues $\lambda_1^* \geq \dots \geq \lambda_p^*$.

Similarly to the classical setting, we then have the expansion $\mathbf{x}^c(t) = \sum_{j=1}^p \mathbf{e}_j^* s_j(t)$, where $s_j(t)$ is the j th score function, defined by $s_j(t) = \mathbf{e}_j^{*T} \mathbf{x}^c(t)$, and it follows straightforwardly from this definition that the CT covariance matrix (3) of $[s_1(t), \dots, s_p(t)]^T$ is $\text{Diag}(\lambda_1^*, \dots, \lambda_p^*)$. Assuming that (8) holds, since each component of $\mathbf{x}^c(t)$ is a linear combination of the basis functions $\phi_1(t), \dots, \phi_K(t)$, the same is true for each of the scores $s_1(t), \dots, s_p(t)$.

Canonical correlation analysis (CCA) is another classical MVA method that is somewhat related to PCA. Here one has two sets of variables and seeks pairs of linear combinations, one for each set, having maximal correlation in an iterative sense. A continuous-time version of CCA is described in Appendix C.

5 Fisher's linear discriminant analysis

In its classical form, Fisher's linear discriminant analysis (LDA) seeks linear combinations $\mathbf{v}^T \mathbf{x}$ that optimally separate $G \geq 2$ sets of observations into which the data set is divided *a priori*. Let $\mathbf{X}_1, \dots, \mathbf{X}_G$ be these sets of observations, where, for $g = 1, \dots, G$, \mathbf{X}_g is $n_g \times p$ with i th row \mathbf{x}_{gi}^T ; let

$$\mathbf{X} = \begin{bmatrix} \mathbf{X}_1 \\ \vdots \\ \mathbf{X}_G \end{bmatrix}$$

be the $n \times p$ combined data set, where $n = n_1 + \dots + n_G$; and let $\bar{\mathbf{x}} = n^{-1} \mathbf{X}^T \mathbf{1}_n$ and $\bar{\mathbf{x}}_g = n_g^{-1} \mathbf{X}_g^T \mathbf{1}_{n_g}$ denote the overall and group- g mean vectors. Like PCA and CCA, Fisher's LDA can be posed as an iterative optimization problem, in this case based on a partition of the total sums of squares and cross-products matrix $\mathbf{T} = n\mathbf{S} = \sum_{g=1}^G \sum_{i=1}^{n_g} (\mathbf{x}_{gi} - \bar{\mathbf{x}})(\mathbf{x}_{gi} - \bar{\mathbf{x}})^T$ into *within-groups* and *between-groups* components, $\mathbf{T} = \mathbf{W} + \mathbf{B}$, where

$$\mathbf{W} = \sum_{g=1}^G \sum_{i=1}^{n_g} (\mathbf{x}_{gi} - \bar{\mathbf{x}}_g)(\mathbf{x}_{gi} - \bar{\mathbf{x}}_g)^T, \quad \mathbf{B} = \sum_{g=1}^G n_g (\bar{\mathbf{x}}_g - \bar{\mathbf{x}})(\bar{\mathbf{x}}_g - \bar{\mathbf{x}})^T.$$

With these definitions, $\mathbf{v}^T \mathbf{W} \mathbf{v}$ is the sum of squared deviations of the linear combinations $\mathbf{v}^T \mathbf{x}_{gi}$ from their within-group means, while $\mathbf{v}^T \mathbf{B} \mathbf{v}$ is a weighted sum of these within-group means from the overall mean, with weight n_g for group g . (Some authors formulate

Fisher's LDA differently, with these weights omitted. Moreover, some authors divide \mathbf{W} and \mathbf{B} by constants that allow them to be interpreted as within- and between-group covariance matrices, but this does not change the solution.) The linear combination $\mathbf{v}_1^T \mathbf{x}$ where $\mathbf{v}_1 = \arg \max_{\mathbf{v}} \mathbf{v}^T \mathbf{B} \mathbf{v} / \mathbf{v}^T \mathbf{W} \mathbf{v}$ can be said to maximally separate the groups, relative to the within-group variation. It can be shown that \mathbf{v}_1 is the eigenvector of $\mathbf{W}^{-1} \mathbf{B}$ corresponding to its largest eigenvalue. If s ($\leq \min\{G - 1, p\}$) is the number of positive eigenvalues of $\mathbf{W}^{-1} \mathbf{B}$, then for $m = 2, \dots, s$, \mathbf{v}_m , the maximizer of $\mathbf{v}^T \mathbf{B} \mathbf{v} / \mathbf{v}^T \mathbf{W} \mathbf{v}$ subject to $\mathbf{v}^T \mathbf{W} \mathbf{v}_1 = \dots = \mathbf{v}^T \mathbf{W} \mathbf{v}_{m-1} = 0$, is given by the eigenvector of $\mathbf{W}^{-1} \mathbf{B}$ corresponding to its m th-largest eigenvalue. The linear combinations $\mathbf{v}_1^T \mathbf{x}, \dots, \mathbf{v}_s^T \mathbf{x}$, which optimally separate the groups in the above iterative sense, are known as Fisher's linear discriminants.

We propose a continuous-time variant of Fisher's linear discriminant analysis that optimally discriminates among $G \geq 2$ subintervals $\mathcal{I}_1, \dots, \mathcal{I}_G$ into which \mathcal{I} is partitioned. For $g \in \{1, \dots, G\}$, let $\bar{\mathbf{x}}_g^* = \mathbf{C}^T \bar{\phi}_g^* = |\mathcal{I}_g|^{-1} \int_{\mathcal{I}_g} \mathbf{x}(t) dt$. Analogously to the classical setting, we have the decomposition $\mathbf{T}^* = \mathbf{W}^* + \mathbf{B}^*$, where

$$\begin{aligned} \mathbf{T}^* &= \int_{\mathcal{I}} [\mathbf{x}(t) - \bar{\mathbf{x}}^*][\mathbf{x}(t) - \bar{\mathbf{x}}^*]^T dt, \\ \mathbf{W}^* &= \sum_{g=1}^G \int_{\mathcal{I}_g} [\mathbf{x}(t) - \bar{\mathbf{x}}_g^*][\mathbf{x}(t) - \bar{\mathbf{x}}_g^*]^T dt, \\ \mathbf{B}^* &= \sum_{g=1}^G |\mathcal{I}_g| (\bar{\mathbf{x}}_g^* - \bar{\mathbf{x}}^*)(\bar{\mathbf{x}}_g^* - \bar{\mathbf{x}}^*)^T. \end{aligned}$$

The CT Fisher's linear discriminants are then functions $\mathbf{v}_1^T \mathbf{x}(t), \dots, \mathbf{v}_s^T \mathbf{x}(t)$ where, similarly to the classical setting, $\mathbf{v}_1, \dots, \mathbf{v}_s$ are eigenvectors of $\mathbf{W}^{*-1} \mathbf{B}^*$ corresponding to the positive eigenvalues in descending order.

Once again, our implementation relies on the basis representation (1) along with (5). Letting $\bar{\phi}_g^* = |\mathcal{I}_g|^{-1} \int_{\mathcal{I}_g} \phi(t) dt$ and $\mathbf{M}_g = |\mathcal{I}_g|^{-1} \int_{\mathcal{I}_g} [\phi(t) - \bar{\phi}_g^*][\phi(t) - \bar{\phi}_g^*]^T dt$, we have

$$\begin{aligned} \mathbf{T}^* &= |\mathcal{I}| \mathbf{C}^T \mathbf{M} \mathbf{C}, \\ \mathbf{W}^* &= \mathbf{C}^T \left(\sum_{g=1}^G |\mathcal{I}_g| \mathbf{M}_g \right) \mathbf{C}, \\ \mathbf{B}^* &= \mathbf{C}^T \left[\sum_{g=1}^G |\mathcal{I}_g| (\bar{\phi}_g^* - \bar{\phi}^*)(\bar{\phi}_g^* - \bar{\phi}^*)^T \right] \mathbf{C}. \end{aligned}$$

6 k -means clustering

Our continuous-time extension of k -means clustering (Hartigan and Wong, 1979) partitions \mathcal{I} into *temporal clusters*, each of which is a subinterval, or a finite union of subintervals, of \mathcal{I} , via the following algorithm:

1. Randomly select centers $\mathbf{m}_1, \dots, \mathbf{m}_k \in \mathbb{R}^p$, perhaps by evaluating $\mathbf{x}(t)$ at k randomly chosen time points.
2. Until a convergence criterion is met:
 - (a) Partition \mathcal{I} into clusters $\mathcal{C}_1, \dots, \mathcal{C}_k$ defined by

$$\mathcal{C}_i = \{t \in \mathcal{I} : d_i(t) < d_j(t) \text{ for all } j \neq i\}$$

for each i , where $d_i(t) = \|\mathbf{x}(t) - \mathbf{m}_i\|$.

- (b) For $i = 1, \dots, k$, update $\mathbf{m}_i = |\mathcal{C}_i|^{-1} \int_{\mathcal{C}_i} \mathbf{x}(t) dt$.

The nontrivial part is step 2(a). As shown in Appendix D, finding the cluster center nearest to $\mathbf{x}(t)$ reduces to finding the $i \in \{1, \dots, k\}$ that minimizes

$$A_i(t) = -2\phi(t)^T \mathbf{C} \mathbf{m}_i + \mathbf{m}_i^T \mathbf{m}_i. \quad (10)$$

Suppose for simplicity that $k = 2$. Then each of $\mathcal{C}_1 = \{t \in \mathcal{I} : A_1(t) < A_2(t)\}$ and $\mathcal{C}_2 = \{t \in \mathcal{I} : A_1(t) > A_2(t)\}$ is a union of subintervals of \mathcal{I} , where the boundaries between these subintervals are the points t at which $A_1(t)$ and $A_2(t)$ cross, i.e., the zero crossings of

$$A_1(t) - A_2(t) = 2\phi(t)^T \mathbf{C} (\mathbf{m}_2 - \mathbf{m}_1) + \mathbf{m}_1^T \mathbf{m}_1 - \mathbf{m}_2^T \mathbf{m}_2. \quad (11)$$

If the basis functions are cubic splines then (11) is a cubic polynomial in t on each of the intervals between knots. Thus finding the transition points between the two clusters reduces to finding, for the cubic polynomial on each of these intervals, any zero crossings that occur within that interval. A formula for the polynomial coefficients is provided in Appendix E. In this way the problem of partitioning infinitely many time points among k clusters is reduced to identifying the zeros of a finite set of polynomials. Thus, for high-temporal-resolution data, CT k -means is potentially much more computationally efficient

than conventional k -means clustering of discrete observations. The $k > 2$ case is similar, but not every crossing point of any pair of $A_i(t)$'s is then a transition point.

7 Examples

7.1 Daily average precipitation in Canada

The simulation results referred to in §2.2 suggest that CT correlations are sometimes stronger than ordinary correlations. As a real-data illustration of this phenomenon, we consider the Canadian precipitation data of Ramsay and Silverman (2005). As in Figure 2, the data consist of daily values for the 35 Canadian weather stations, but here the variable of interest is base-10 log of the average precipitation in millimeters (see Ramsay et al., 2023). Figure 3 displays the data in raw form (upper panel) and after smoothing (middle panel), using the same strategy as for the temperature data in Figure 2. The lower left panel of Figure 3 presents the ordinary Pearson correlation among the 35 stations' precipitation levels, when the data are treated as $n = 365$ discrete observations of $p = 35$ variables.

The lower right panel shows the CT correlations based on the smooth curves. The CT correlations are much stronger than raw correlations, and preliminary simulation results (see §2.2) support viewing the former as more accurate than the latter. For each correlation matrix, the stations are ordered by the angles formed by the leading two eigenvectors; this ordering helps to reveal patterns and groupings among the correlations (Friendly and Kwan, 2003). In both correlation matrices the reordering puts the same nine stations at the end: the first six of the original ordering, which are located on the Atlantic coast, along with Vancouver, Victoria and Prince Rupert, on the Pacific coast. The CT correlation matrix suggests that these nine stations form a tight cluster, with positive correlations among them and negative correlations between them and the inland stations. This pattern is much less clear in the ordinary correlation matrix, due perhaps to the attenuation phenomenon noted in §2.2. As can be seen in the middle panel of Figure 3, the Atlantic and Pacific stations tend to have the least precipitation in the summer, while the inland stations have an

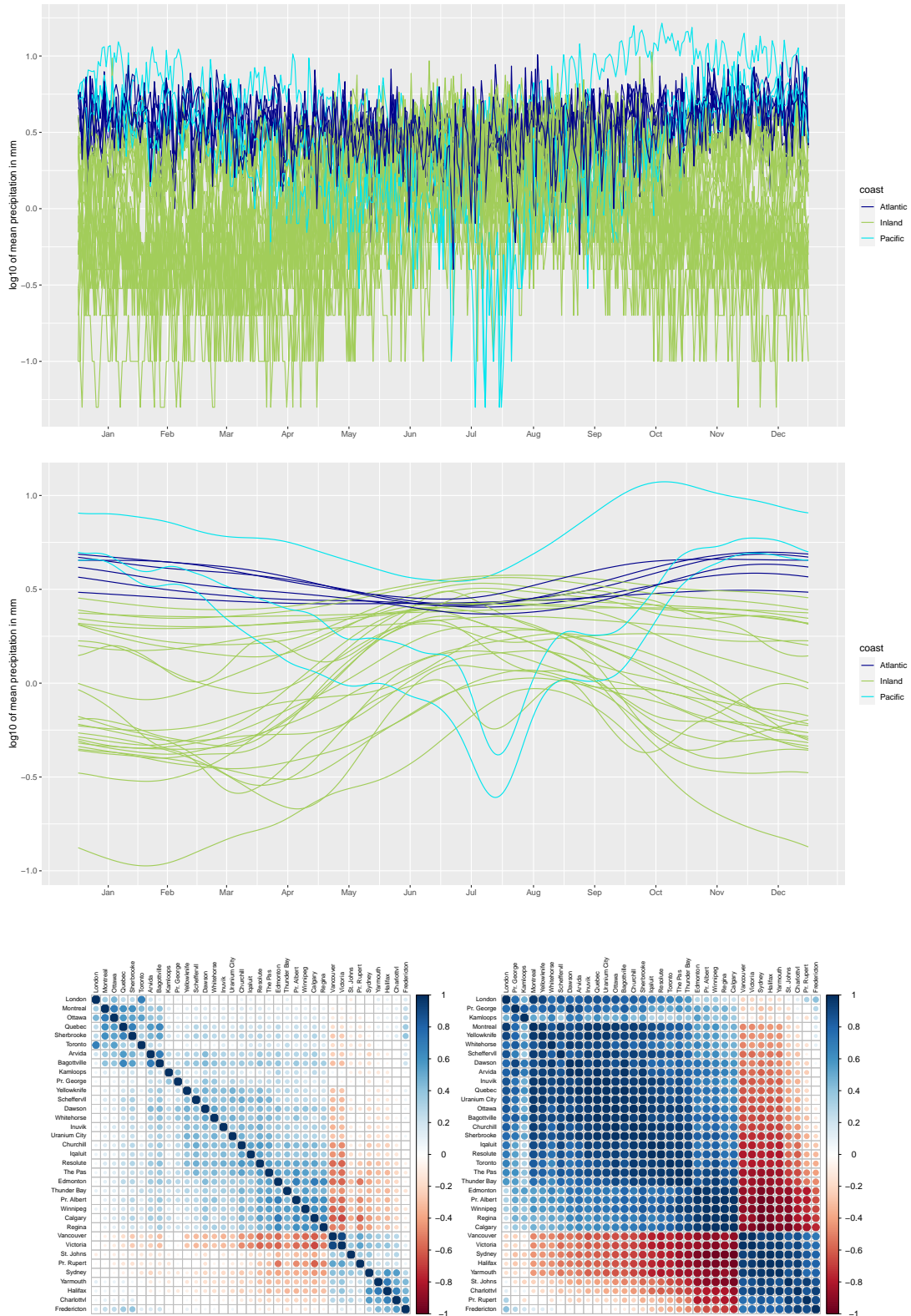


Figure 3: Base-10 log mean daily precipitation in mm for the 35 Canadian weather stations of Ramsay and Silverman (2005), in raw form₁₅ (above) and after smoothing (middle). Below: Correlations among the 35 weather stations, obtained by treating the data as $n = 365$ discrete observations (left) and by the continuous-time approach (right).

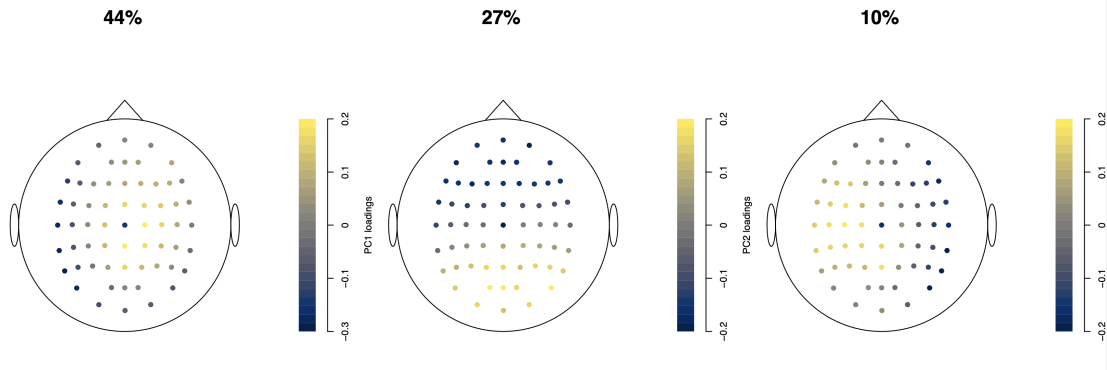


Figure 4: Loadings of the first three continuous-time principal components for an example EEG trial. panel titles give the percent variance explained by each PC.

opposite pattern.

We remark that Ramsay and Silverman (2005), as well as R package `fda` (Ramsay et al., 2023) and a number of subsequent analyses of the Canadian weather data, divide the stations into four regions, including 15 “Atlantic” and 5 “Pacific” stations. The nine stations referred to in the previous paragraph meet a stricter criterion of proximity to the Atlantic or Pacific, as shown on the map in Appendix F.

7.2 Electroencephalography data

We applied continuous-time PCA to a portion of the Begleiter electroencephalography (EEG) data set from the UCI Machine Learning Repository, made available in R by Helwig (2018). The data consist of multiple EEG trials for each of a set of individuals, with each trial consisting of electrical signals at $p = 64$ channels with 256 time points within 1 second. Loadings for the first 3 PCs for a randomly selected trial are shown in Figure 4, and these have reasonably clear interpretations: PC1 roughly captures the balance between signal in brain regions that are more central versus more peripheral (as viewed from above), PC2 represents anterior versus posterior regions, and PC3 represents left versus right hemisphere.

A natural next step would be multilevel CT-PCA to analyze multiple trials nested within individuals, as are available with this data set. The aim would be similar to the

multilevel, longitudinal and structured variants of functional PCA (Di et al., 2009; Greven et al., 2010; Shou et al., 2013, 2015; Cui et al., 2023), but rather than decomposing a covariance operator, the structure being decomposed is a $p \times p$ covariance or correlation matrix as in Timmerman and Kiers (2002). We leave this development to future work.

7.3 Chicago air pollution

Wood (2017) performed several analyses relating air pollution to death rates, using a data set of daily indicators for Chicago for the years 1987 to 2000 made available by Peng and Welty (2004). Here we focus on the four predictors in these analyses, namely PM_{10} (median 2.5- to 10- μm particles per m^3), ozone (in parts per billion), SO_2 (median sulfur dioxide measurement), and temperature. Our goal here is exploratory analyses of these four metrics using two CTMVA methods. All four variables were standardized and were smoothed using a 200-dimensional B -spline basis and AR(1) residuals (Wood, 2017).

Figure 5 displays results from continuous-time 3-means clustering. The upper panel shows the four standardized variables' time series with vertical lines indicating transitions among the three clusters. As can be discerned more clearly in the lower panel, which shows the clustering separately by year, there is a fairly consistent seasonal pattern: cluster 1 corresponds roughly to the winter, cluster 2 to the summer, and cluster 3 to the spring and autumn. Thus, with one exception, each calendar year is divided into portions belonging to clusters 1, 3, 2, 3, 1, in that order. The only exception is the winter of 1991-92, in which cluster 1 does not appear. The strong seasonal pattern seems to be driven largely by temperature variations, along with the high positive correlations of PM_{10} and ozone with temperature. SO_2 , on the other hand, is quite negatively correlated with temperature. In the winter of 1991-92, however, SO_2 uncharacteristically dropped along with the other three variables, and this may help explain the non-occurrence of cluster 1. We note that when ordinary 3-means clustering is applied to the raw time series, there are over 1100 transitions among the resulting three clusters, making it difficult at best to detect the cyclic seasonal pattern that emerges clearly from the continuous-time analysis.

Another way to compare and contrast the different years in this data set is via continuous-

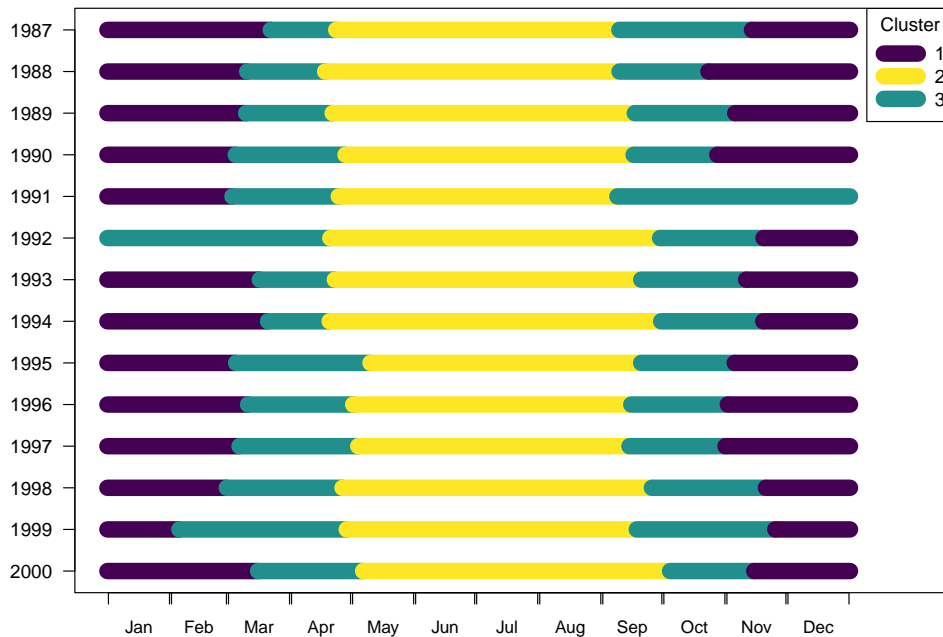
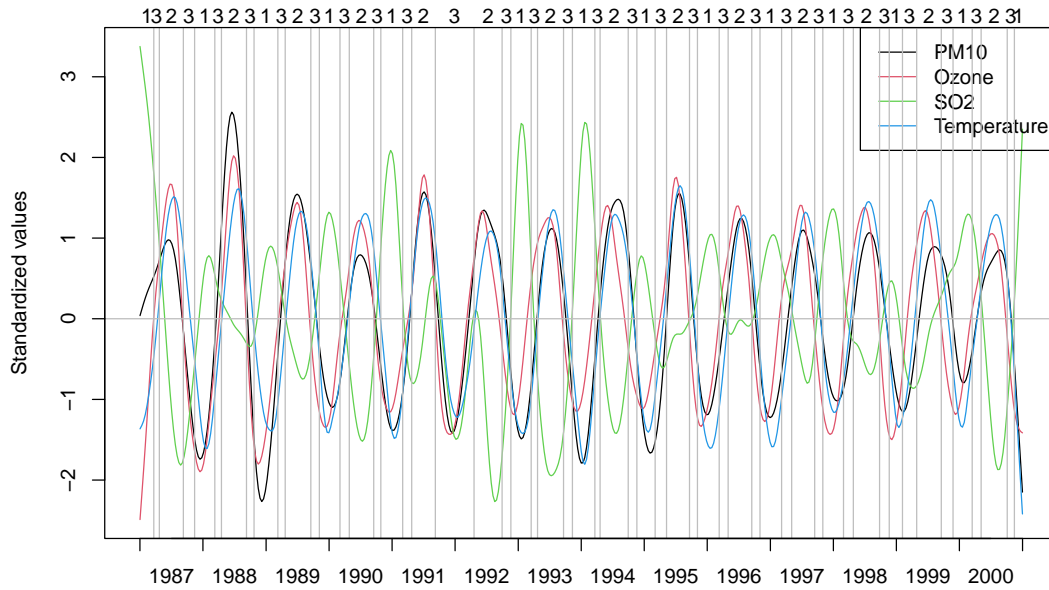


Figure 5: Above: The four standardized variables from the Chicago air pollution data. Vertical lines indicate transitions among the clusters found by CT 3-means clustering, with cluster numbers shown along the top of the plot. Below: The same cluster transitions displayed separately by year.

	LD ₁	LD ₂	LD ₃	LD ₄
PM ₁₀	0.0302	-0.0235	0.0001	-0.0031
Ozone	-0.0037	0.0134	-0.0203	-0.0062
SO ₂	-0.0186	-0.0105	-0.0054	-0.0002
Temperature	-0.0380	0.0034	0.0167	-0.0058

Table 1: Coefficients of Fisher’s linear discriminants for the Chicago air pollution data.

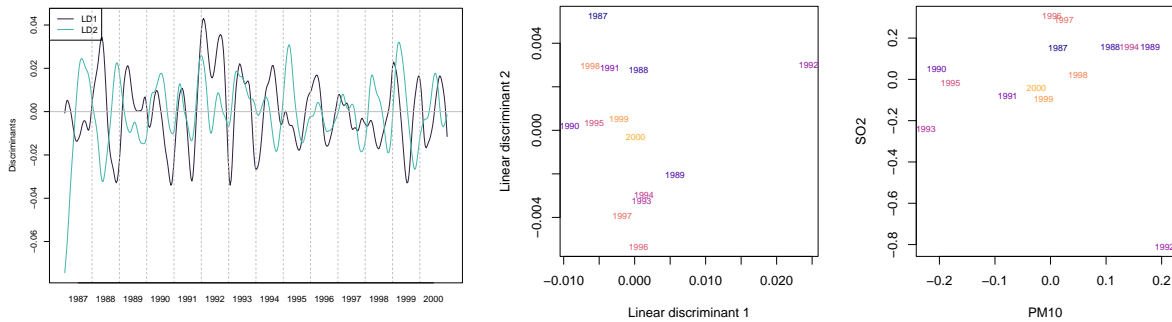


Figure 6: Left: The first two linear discriminants for the Chicago air pollution data, displayed as functions of date. Center: Mean values of the first two discriminants for each of the 14 years. Right: Mean PM₁₀ and mean SO₂ for each year.

time Fisher’s linear discriminant analysis, with the $G = 14$ calendar years as subintervals among which we wish to discriminate. The four linear discriminants that result have coefficient vectors $\mathbf{v}_1, \mathbf{v}_2, \mathbf{v}_3, \mathbf{v}_4$ given in Table 1. The plot of the time series of the first two discriminants in Figure 6 suggests that, as in the cluster analysis, the year 1992 stands out: the value of LD₁ tends to be very high during that year. This impression is confirmed by the middle panel, which shows the average values of the first two discriminants in each year and reveals that 1992 is a clear outlier for LD₁. This finding is explained by the very high mean PM₁₀ and extremely low mean SO₂ for 1992, as seen in the right panel.

8 Discussion

The data sets in our illustrations of CTMVA can be handled by classical MVA methods, which are commonly applied to multivariate time series (e.g., Jolliffe, 2002). But our preliminary simulation study summarized in §2.2, and the 3-means cluster analysis in §7.3 suggest that the denoised, smooth representation in CTMVA can, at least in some cases, lead to improved performance over standard MVA with the raw data. In addition, as noted in the Introduction, CTMVA can be applied in certain settings for which classical MVA is unavailable, such as variables with disparate measurement times. Another such setting is correlated point processes, such as inhomogeneous Poisson processes. Ramsay and Silverman (2005) present a smooth basis function approach to estimating a time-varying intensity function $\iota(t)$. Given p inhomogeneous Poisson processes with intensities $\iota_1(t), \dots, \iota_p(t)$ on a common time interval, one can compute CT correlations among estimates of these intensities. However, more work is required on reliable smoothing parameter estimation for intensity functions.

Another aim of future work is to develop *multilevel CTMVA* for large data sets consisting of multiple instances of continuous-time multivariate data, such as the full EEG data set referred to in §7.2. This may be contrasted with two complex data structures extending the $n \times \infty$ setup of traditional FDA: *multilevel* and *multivariate* FDA. Heuristically, multilevel FDA (e.g. Crainiceanu et al., 2009, 2011) considers $(n \times m) \times \infty$ data, in which a given function is observed m times in each of n individuals, whereas multivariate functional data (e.g. Berrendero et al., 2011; Chiou and Müller, 2014) can be thought of as $n \times (v \times \infty)$, with n instances of a collection of v functions. (These three-way “dimensionalities” are oversimplifications: multilevel functional data need not have exactly m repetitions per subject, and multivariate functional data may consist of v functions on different domains (e.g. Happ and Greven, 2018).) The multilevel CTMVA setup, of multiple instances of $\infty \times p$ data, differs from the either multilevel or multivariate FDA and may be more similar to the setup of Dubin and Müller (2005). But whereas these authors estimate population dynamical correlation from a sample of $\infty \times p$ -type observations, the aim of multilevel CT correlation would be to decompose the correlations among p variables into “within”

and “between” components. Multilevel data will also allow for assessing the reliability of CTMVA results, via extensions of intraclass correlation (Shou et al., 2013; Xu et al., 2021).

The proposed methods are implemented in the R package `ctmva` (Reiss and Paul, 2023).

APPENDICES

A Computing (5)

It is readily shown that the matrix $\mathbf{M} = |\mathcal{I}|^{-1} \int_{\mathcal{I}} [\boldsymbol{\phi}(t) - \bar{\boldsymbol{\phi}}^*][\boldsymbol{\phi}(t) - \bar{\boldsymbol{\phi}}^*]^T dt$ of (5) can be written as

$$\mathbf{M} = |\mathcal{I}|^{-1} \mathbf{G} - \bar{\boldsymbol{\phi}}^* \bar{\boldsymbol{\phi}}^{*T},$$

where $\mathbf{G} = \int_{\mathcal{I}} \boldsymbol{\phi}(t) \boldsymbol{\phi}(t)^T dt$, i.e., the $K \times K$ matrix with (k, ℓ) element $g_{k\ell} = \int_{\mathcal{I}} \phi_k(t) \phi_\ell(t) dt$.

If $\boldsymbol{\phi}$ is an orthonormal Fourier basis on \mathcal{I} then $\mathbf{G} = \mathbf{I}_K$ and $\bar{\boldsymbol{\phi}}^* = (|\mathcal{I}|^{-1/2}, 0, \dots, 0)^T$, so that \mathbf{M} is simply the diagonal matrix with main diagonal $(0, |\mathcal{I}|^{-1}, \dots, |\mathcal{I}|^{-1})^T$.

For a B -spline basis, $\bar{\boldsymbol{\phi}}^*$ and \mathbf{G} are obtained by numerical integration, with quadrature points t_1, \dots, t_Q and corresponding weights w_1, \dots, w_Q . Let $\boldsymbol{\Phi}$ be the $Q \times K$ matrix of evaluation of the basis functions at the quadrature points, i.e., the (q, k) entry of $\boldsymbol{\Phi}$ is $\phi_k(t_q)$. For basis objects in the R package `fd` (Ramsay et al., 2023), this matrix can be generated with a call to function `eval.basis` from that package. Let \mathbf{W} be the $Q \times Q$ diagonal matrix whose diagonal elements are the quadrature weights. Then for $k = 1, \dots, K$, $\boldsymbol{\Phi}^T \mathbf{W} \mathbf{1}_Q$ has k th element $\sum_{q=1}^Q w_q \phi_k(t_q) \approx \int_{\mathcal{I}} \phi_k(t) dt$ and thus

$$\bar{\boldsymbol{\phi}}^* \approx |\mathcal{I}|^{-1} \boldsymbol{\Phi}^T \mathbf{W} \mathbf{1}_Q.$$

Similarly, $\boldsymbol{\Phi}^T \mathbf{W} \boldsymbol{\Phi}$ has (k, ℓ) element $\sum_{q=1}^Q w_q \phi_k(t_q) \phi_\ell(t_q) \approx \int_{\mathcal{I}} \phi_k(t) \phi_\ell(t) dt$, and thus

$$\mathbf{G} \approx \boldsymbol{\Phi}^T \mathbf{W} \boldsymbol{\Phi}.$$

Our implementation uses the the Newton-Cotes 7-point rule for numerical quadrature, as suggested by Wand and Ormerod (2008). For cubic or lower-order B -splines, the Newton-Cotes 7-point rule makes the above integrals exact rather than approximate, so that \mathbf{M} is obtained exactly.

B Diagnosing the need for detrending

We present here a simple diagnostic to indicate, for a given data set, whether removing a common trend before computing the CT covariance or correlation (see §3) would be

beneficial. If we adopt an FDA viewpoint toward the p functions $x_1(t), \dots, x_p(t)$, a strong common trend implies that all p functions are quite similar to an underlying mean function $\mu_x(t)$. This similarity can be quantified by using the function `pffr` (Ivanescu et al., 2015; Scheipl et al., 2015) from the R package `refund` (Goldsmith et al., 2023) to fit the simplest possible functional-response model, namely $x_i(t) = \mu_x(t) + \varepsilon_i(t)$ for $i = 1, \dots, p$. Here $\mu_x(t)$ is a “functional intercept,” in line with the syntax for this model, `pffr(X ~ 1)` where \mathbf{X} is a p -row matrix containing the functions. The (adjusted) R^2 outputted by `pffr` for this model (based on the underlying model fitted by the R package `mgcv` of Wood, 2017) gives the variance explained, for the collection of all points $x_i(t)$ in all p functions, by the fitted values $\hat{x}_i(t) = \hat{\mu}_x(t)$. This “pointwise” R^2 (as opposed to the *functional* R^2 of Müller and Yao, 2008, which equals zero for this model) provides a measure of the strength of the common trend. For the Canadian weather data set, R^2 is found to be 71% for the temperature curves, but only 4.9% for the log precipitation curves; hence our decision to detrend the former (see §3) but not the latter (see §7.1).

C Continuous-time canonical correlation analysis

In classical canonical correlation analysis (CCA) we are given an $n \times p$ matrix \mathbf{X} and an $n \times q$ matrix \mathbf{Y} , and we seek *pairs* of unit vectors $\mathbf{a} \in \mathbb{R}^p, \mathbf{b} \in \mathbb{R}^q$ such that the sample correlation of $\mathbf{a}^T \mathbf{x}, \mathbf{b}^T \mathbf{y}$ is maximized in an iterative sense:

1. $\mathbf{a}_1^T \mathbf{x}, \mathbf{b}_1^T \mathbf{y}$ attain the maximal sample correlation among all pairs (\mathbf{a}, \mathbf{b}) of unit vectors $\mathbf{a} \in \mathbb{R}^p, \mathbf{b} \in \mathbb{R}^q$.
2. For $m = 2, \dots, \min\{p, q\}$, $\mathbf{a}_m^T \mathbf{x}, \mathbf{b}_m^T \mathbf{y}$ attain the maximal sample correlation among all pairs (\mathbf{a}, \mathbf{b}) of unit vectors such that $\mathbf{a}^T \mathbf{x}$ is uncorrelated with $\mathbf{a}_1^T \mathbf{x}, \dots, \mathbf{a}_{m-1}^T \mathbf{x}$ and $\mathbf{b}^T \mathbf{y}$ is uncorrelated with $\mathbf{b}_1^T \mathbf{y}, \dots, \mathbf{b}_{m-1}^T \mathbf{y}$.

Then $(\mathbf{a}_m^T \mathbf{x}, \mathbf{b}_m^T \mathbf{y})$ are the m th pair of canonical variables, and their correlation is the m th canonical correlation.

The solution to the iterative maximization problem is given in terms of the covariance

matrices of the two sets of variables, as well as their cross-covariance matrix:

$$\mathbf{S}_{xx} = n^{-1} \mathbf{X}^{cT} \mathbf{X}^c, \quad \mathbf{S}_{yy} = n^{-1} \mathbf{Y}^{cT} \mathbf{Y}^c, \quad \mathbf{S}_{xy} = n^{-1} \mathbf{X}^{cT} \mathbf{Y}^c, \quad \mathbf{S}_{yx} = \mathbf{S}_{xy}^T,$$

where $\mathbf{X}^c, \mathbf{Y}^c$ are column-centered versions of the two matrices and $\mathbf{S}_{xx}, \mathbf{S}_{xy}$ are assumed to be nonsingular. It can be shown (e.g., Rencher and Christensen, 2012) that

$$\mathbf{M}_1 = \mathbf{S}_{xx}^{-1} \mathbf{S}_{xy} \mathbf{S}_{yy}^{-1} \mathbf{S}_{yx} \quad \text{and} \quad \mathbf{M}_2 = \mathbf{S}_{yy}^{-1} \mathbf{S}_{yx} \mathbf{S}_{xx}^{-1} \mathbf{S}_{xy}$$

have the same positive eigenvalues $r_1^2 \geq r_2^2 \geq \dots \geq r_{\min\{p,q\}}^2$, and that if $\mathbf{a}_i, \mathbf{b}_i$ are eigenvectors of $\mathbf{M}_1, \mathbf{M}_2$ respectively corresponding to the i th largest eigenvalue, then $\mathbf{a}_i^T \mathbf{x}$, $\mathbf{b}_i^T \mathbf{y}$ are the i th canonical variates, with canonical correlation r_i , which can be forced to be positive by multiplying either \mathbf{a}_i or \mathbf{b}_i by -1 if needed.

To develop a continuous-time version of CCA, suppose that two sets of functions, $\mathbf{x}(t) = [x_1(t), \dots, x_p(t)]^T$ and $\mathbf{y}(t) = [y_1(t), \dots, y_q(t)]^T$, are defined on \mathcal{I} . We now seek pairs (\mathbf{a}, \mathbf{b}) of unit vectors defining linear combinations $\mathbf{a}^T \mathbf{x}(t), \mathbf{b}^T \mathbf{y}(t)$ of the two sets of functions that have maximal correlation in the above iterative sense, but here, generalizing (9), the covariance of $\mathbf{a}^T \mathbf{x}(t), \mathbf{b}^T \mathbf{y}(t)$ is given by

$$|\mathcal{I}|^{-1} \int_{\mathcal{I}} [\mathbf{a}^T \{\mathbf{x}(t) - \bar{\mathbf{x}}\}] [\mathbf{b}^T \{\mathbf{y}(t) - \bar{\mathbf{y}}\}] dt$$

and their correlation is then given by

$$\frac{\int_{\mathcal{I}} [\mathbf{a}^T \{\mathbf{x}(t) - \bar{\mathbf{x}}\}] [\mathbf{b}^T \{\mathbf{y}(t) - \bar{\mathbf{y}}\}] dt}{\sqrt{\int_{\mathcal{I}} [\mathbf{a}^T \{\mathbf{x}(t) - \bar{\mathbf{x}}\}]^2 dt \int_{\mathcal{I}} [\mathbf{b}^T \{\mathbf{y}(t) - \bar{\mathbf{y}}\}]^2 dt}}.$$

These pairs of linear combinations may be called the *canonical functions*.

We assume for simplicity that both sets of functions are represented with respect to a common K -dimensional basis $\boldsymbol{\phi}$, i.e.,

$$\mathbf{x}(t) = \mathbf{C}_x^T \boldsymbol{\phi}(t), \quad \mathbf{y}(t) = \mathbf{C}_y^T \boldsymbol{\phi}(t)$$

for some matrices $\mathbf{C}_x, \mathbf{C}_y$ of dimension $K \times p, K \times q$ respectively. As with PCA, the continuous-time solution to the iterative maximization problem ensues upon “translating” the relevant matrices to the continuous-time setting. We do so by defining

$$\mathbf{M}_1^* = \mathbf{S}_{xx}^{*-1} \mathbf{S}_{xy}^* \mathbf{S}_{yy}^{*-1} \mathbf{S}_{yx}^* \quad \text{and} \quad \mathbf{M}_2^* = \mathbf{S}_{yy}^{*-1} \mathbf{S}_{yx}^* \mathbf{S}_{xx}^{*-1} \mathbf{S}_{xy}^*,$$

where

$$\mathbf{S}_{xx}^* = \mathbf{C}_x^T \mathbf{M} \mathbf{C}_x, \quad \mathbf{S}_{yy}^* = \mathbf{C}_y^T \mathbf{M} \mathbf{C}_y, \quad \mathbf{S}_{xy}^* = \mathbf{C}_x^T \mathbf{M} \mathbf{C}_y^T, \quad \mathbf{S}_{yx}^* = \mathbf{S}_{xy}^{*T},$$

with \mathbf{M} defined as in (5). Then, as in the classical case, $\mathbf{M}_1^*, \mathbf{M}_2^*$ have the same positive eigenvalues; and if $\mathbf{a}_i, \mathbf{b}_i$ are eigenvectors of $\mathbf{M}_1^*, \mathbf{M}_2^*$ respectively corresponding to the i th largest eigenvalue, then $\mathbf{a}_i^T \mathbf{x}(t), \mathbf{b}_i^T \mathbf{y}(t)$ are the i th canonical functions.

D Derivation of (10)

By (1), the squared distance from $\mathbf{x}(t)$ to the cluster- i center is

$$\begin{aligned} d_i(t)^2 &= \|\mathbf{C}^T \boldsymbol{\phi}(t) - \mathbf{m}_i\|^2 \\ &= \boldsymbol{\phi}(t)^T \mathbf{C} \mathbf{C}^T \boldsymbol{\phi}(t) + A_i(t) \end{aligned} \tag{A12}$$

where $A_i(t) = -2\boldsymbol{\phi}(t)^T \mathbf{C} \mathbf{m}_i + \mathbf{m}_i^T \mathbf{m}_i$ as in (10). Since the first term in (A12) does not depend on i , it follows that for a given t , the cluster number i for which $A_i(t)$ is minimized is also the one for which $d_i(t) = \|\mathbf{x}(t) - \mathbf{m}_i\|$ is minimized, as claimed.

E A formula for (11) in the cubic spline case

If the basis $\boldsymbol{\phi}(t)$ consists of cubic splines then, within the j th inter-knot interval (for $j = 1, \dots, K - 3$; see Ramsay and Silverman, 2005), $\boldsymbol{\phi}(t)^T = (1 \ t \ t^2 \ t^3) \mathbf{L}_j$ for a $4 \times K$ matrix \mathbf{L}_j of polynomial coefficients. Substituting this into (11), we conclude that $A_1(t) - A_2(t) = (1 \ t \ t^2 \ t^3) \mathbf{v}_j$ where

$$\mathbf{v}_j = 2\mathbf{L}_j \mathbf{C} (\mathbf{m}_2 - \mathbf{m}_1) + \begin{bmatrix} \mathbf{m}_1^T \mathbf{m}_1 - \mathbf{m}_2^T \mathbf{m}_2 \\ 0 \\ 0 \\ 0 \end{bmatrix}.$$

Consequently, the zeroes of the cubic polynomial (11) in the j th inter-knot interval can be found by inputting this vector \mathbf{v}_j to R function `polyroot`, which implements the Jenkins-Traub zero-finding algorithm.

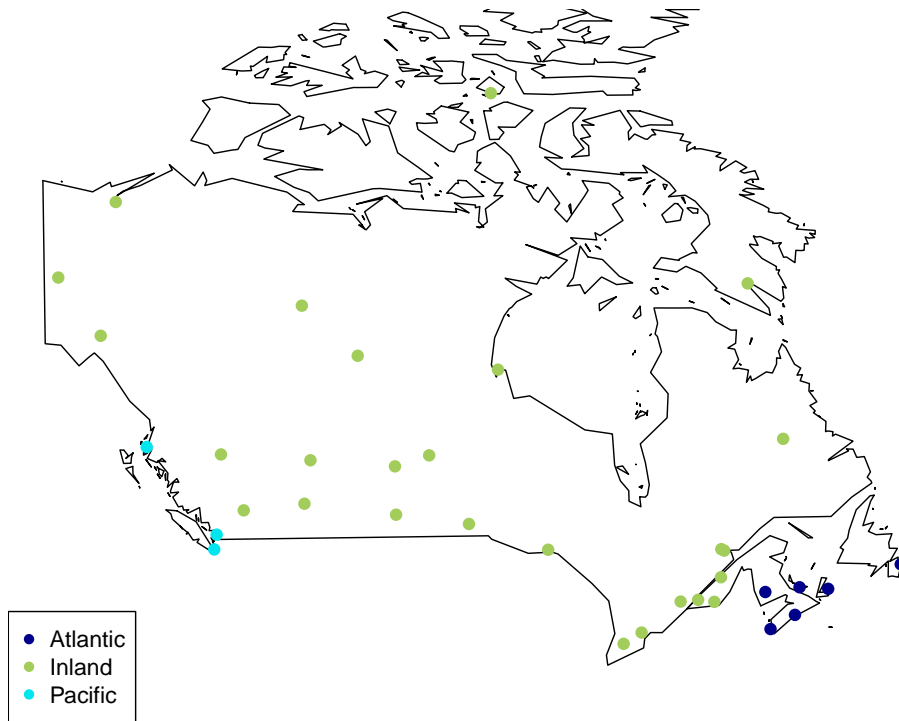


Figure A7: The 35 Canadian weather stations, color-coded by location on the Atlantic or Pacific coast or inland.

F Coastal versus inland weather stations

The CT correlation matrix of the log mean precipitation values for the 35 Canadian weather stations, displayed in Figure 3 of the main text, reveals that the nine coastal stations (six on the Atlantic and three on the Pacific coast) tend to be highly correlated with each other and anticorrelated with the 26 inland stations. Figure A7 provides a map of this division of the 35 weather stations into three subsets, using the same color-coding as in Figure 3 of the main text.

References

- Berrendero, J. R., A. Justel, and M. Svarc (2011). Principal components for multivariate functional data. *Computational Statistics & Data Analysis* 55(9), 2619–2634.
- Chiou, J.-M. and H.-G. Müller (2014). Linear manifold modelling of multivariate functional data. *Journal of the Royal Statistical Society: Series B* 76(3), 605–626.
- Cohen, J., P. Cohen, S. G. West, and L. S. Aiken (2013). *Applied Multiple Regression/Correlation Analysis for the Behavioral Sciences* (3rd ed.). Routledge.
- Crainiceanu, C. M., B. S. Caffo, S. Luo, V. M. Zipunnikov, and N. M. Punjabi (2011). Population value decomposition, a framework for the analysis of image populations. *Journal of the American Statistical Association* 106, 775–790.
- Crainiceanu, C. M., A.-M. Staicu, and C.-Z. Di (2009). Generalized multilevel functional regression. *Journal of the American Statistical Association* 104, 1550–1561.
- Cui, E., R. Li, C. M. Crainiceanu, and L. Xiao (2023). Fast multilevel functional principal component analysis. *Journal of Computational and Graphical Statistics* 32(2), 366–377.
- Di, C.-Z., C. M. Crainiceanu, B. S. Caffo, and N. M. Punjabi (2009). Multilevel functional principal component analysis. *Annals of Applied Statistics* 3(1), 458.
- Dubin, J. A. and H.-G. Müller (2005). Dynamical correlation for multivariate longitudinal data. *Journal of the American Statistical Association* 100, 872–881.
- Friendly, M. (2002). Corrgrams: Exploratory displays for correlation matrices. *The American Statistician* 56(4), 316–324.
- Friendly, M. and E. Kwan (2003). Effect ordering for data displays. *Computational Statistics & Data Analysis* 43(4), 509–539.
- Goldsmith, J., F. Scheipl, L. Huang, J. Wrobel, C. Di, J. Gellar, J. Harezlak, M. W. McLean, B. Swihart, L. Xiao, C. Crainiceanu, and P. T. Reiss (2023). *refund: Regression with Functional Data*. R package version 0.1-30.

- Greven, S., C. Crainiceanu, B. Caffo, and D. Reich (2010). Longitudinal functional principal component analysis. *Electronic Journal of Statistics* 4, 1022–1054.
- Happ, C. and S. Greven (2018). Multivariate functional principal component analysis for data observed on different (dimensional) domains. *Journal of the American Statistical Association* 113, 649–659.
- Hartigan, J. and M. Wong (1979). A k-means clustering algorithm. *Applied Statistics* 28, 100–108.
- Helwig, N. E. (2018). *eegkit: Toolkit for Electroencephalography Data*. R package version 1.0-4.
- Ivanescu, A. E., A.-M. Staicu, F. Scheipl, and S. Greven (2015). Penalized function-on-function regression. *Computational Statistics* 30, 539–568.
- Jolliffe, I. T. (2002). *Principal Component Analysis* (2nd ed.). Springer.
- Mardia, K. V., J. T. Kent, and J. M. Bibby (1979). *Multivariate Analysis*. New York: Academic Press.
- Müller, H.-G. and F. Yao (2008). Functional additive models. *Journal of the American Statistical Association* 103, 1534–1544.
- Peng, R. D. and L. J. Welty (2004). The nmmapsdata package. *R News* 4(2), 10–14.
- R Core Team (2023). *R: A Language and Environment for Statistical Computing*. Vienna, Austria: R Foundation for Statistical Computing.
- Ramsay, J. O. (1982). When the data are functions. *Psychometrika* 47(4), 379–396.
- Ramsay, J. O., G. Hooker, and S. Graves (2009). *Functional Data Analysis with R and MATLAB*. New York: Springer.
- Ramsay, J. O., G. Hooker, and S. Graves (2023). *fda: Functional Data Analysis*. R package version 6.1.4.

- Ramsay, J. O. and B. W. Silverman (2005). *Functional Data Analysis* (2nd ed.). New York: Springer.
- Reiss, P. T. and R. T. Ogden (2009). Smoothing parameter selection for a class of semiparametric linear models. *Journal of the Royal Statistical Society: Series B* 71(2), 505–523.
- Reiss, P. T. and B. Paul (2023). *ctmva: Continuous-time multivariate analysis*. R package version 1.3.
- Rencher, A. C. and W. F. Christensen (2012). *Methods of Multivariate Analysis*. John Wiley & Sons, Inc.
- Ruppert, D., M. P. Wand, and R. J. Carroll (2003). *Semiparametric Regression*. Cambridge, UK: Cambridge University Press.
- Scheipl, F., A.-M. Staicu, and S. Greven (2015). Functional additive mixed models. *Journal of Computational and Graphical Statistics* 24(2), 477–501.
- Schott, J. R. (2017). *Matrix Analysis for Statistics* (3rd ed.). Hoboken, New Jersey: John Wiley & Sons.
- Shou, H., A. Eloyan, S. Lee, V. Zipunnikov, A. Crainiceanu, M. Nebel, B. Caffo, M. Lindquist, and C. M. Crainiceanu (2013). Quantifying the reliability of image replication studies: the image intraclass correlation coefficient (I2C2). *Cognitive, Affective, & Behavioral Neuroscience* 13(4), 714–724.
- Shou, H., V. Zipunnikov, C. M. Crainiceanu, and S. Greven (2015). Structured functional principal component analysis. *Biometrics* 71(1), 247–257.
- Spearman, C. (1910). Correlation calculated from faulty data. *British Journal of Psychology* 3(3), 271–295.
- Timmerman, M. E. and H. A. L. Kiers (2002). Three-way component analysis with smoothness constraints. *Computational Statistics & Data Analysis* 40(3), 447–470.

- Wand, M. P. and J. T. Ormerod (2008). On semiparametric regression with O’Sullivan penalized splines. *Australian & New Zealand Journal of Statistics* 50(2), 179–198.
- Wei, T. and V. Simko (2021). *R package ‘corrplot’: Visualization of a Correlation Matrix*. Version 0.92.
- Wood, S. N. (2011). Fast stable restricted maximum likelihood and marginal likelihood estimation of semiparametric generalized linear models. *Journal of the Royal Statistical Society: Series B* 73(1), 3–36.
- Wood, S. N. (2017). *Generalized Additive Models: An Introduction with R* (2nd ed.). Boca Raton, Florida, USA: CRC Press.
- Xu, M., P. T. Reiss, and I. Cribben (2021). Generalized reliability based on distances. *Biometrics* 77(1), 258–270.